Correction schemes for self-demagnetisation

Dean Hillan
CSIRO Earth Science and Resource Engineering
11 Juilius Ave, North Ryde
NSW, Australia
dean.hillan@csiro.au

Clive Foss
CSIRO Earth Science and Resource Engineering
11 Juilius Ave, North Ryde
NSW, Australia
clive.foss@csiro.au

SUMMARY

Aeromagnetic surveys collected over bodies of high susceptibility record fields that have been significantly affected by self-demagnetisation. These effects complicate interpretation as the amplitude of the magnetic response scales non-linearly with the susceptibility. Analytic modelling is only carried out for compact ellipsoidal bodies and most approaches break down in the high susceptibility limit. It therefore of interest to develop tools for understanding and modelling of self-demagnetisation effects to support geophysical exploration. We present a modelling scheme based on multiple prismatic sub-volume bodies in a 3D grid for investigating and testing self-demagnetisation effects. This scheme, and another recent iterative scheme based on multiple spherical voxels, is tested to demonstrate self-demagnetisation effects on simple bodies. The schemes are verified against the known analytic results for a spherical body and the results for a cubic body. The prismatic scheme is then used to model a dipping magnetite sheet for comparison against real data where self-demagnetisation effects are thought to be important. Finally, we demonstrate the main advantage of the correction scheme by modelling multiple magnetic bodies in a 3D grid. These correction schemes are aimed at improving current magnetic modelling techniques and providing solutions for dealing with complex and highly susceptible bodies.

Key words: Magnetics; Interpretation; Potential fields; Self demagnetisation.

INTRODUCTION

All magnetic bodies demonstrate self-demagnetisation (SDM) to a degree. These effects can reasonably be ignored for bodies with a magnetic susceptibility of less than 0.1 SI. However, the magnitudes of the anomalous fields generated by moderately to highly susceptible bodies (above κ=0.1 SI) do not scale linearly with the inducing field and need to be compensated for to allow accurate subsurface modelling and data interpretation.

Simple bodies may account for the SDM field $\boldsymbol{F_d}$ via a demagnetisation factor $\boldsymbol{N}$ such that

$$\boldsymbol{F_d}=-\boldsymbol{N}\boldsymbol{J_e}\,. \tag{1}$$

The effective magnetisation $\boldsymbol{J_e}$ is then given by

$$\boldsymbol{J_e}=\kappa\boldsymbol{F_0}\,/\,(1+N_i\kappa). \tag{2}$$

The relevant fields are illustrated in Figure 1. Generally N_i is an approximate demagnetisation factor which may have unequal components for each axis or may be a function of susceptibility. For example, a cubic body of low susceptibility (κ<0.1) has N_i=1/3 which decreases towards N_i~0.28 as $\kappa\to\infty$ (Sharma 1966; Eskola et al. 1977). In the case of an ellipsoid it can be shown that the sum of three demagnetisation factor components always add to unity, with the sphere being a special case where N_i=1/3 (Emerson et al. 1985; Clark et al. 1986).

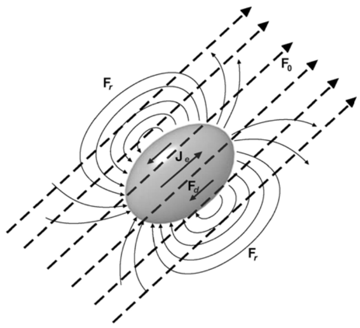

Figure 1. Schematic showing the demagnetising field F_d generated by a body in a uniformly magnetising field F_0. The total internal magnetic field is then $F_d + F_0$. (Purss and Cull 2005).

Calculation of the demagnetisation factor for non-ellipsoidal bodies becomes difficult for κ>1 since edge effects begin to dominate the mean induced secondary field. Another approach is based on dividing the body into many prismatic sub-volumes and calculating the interactions (i.e. Sharma 1966) and more recently the use of spherical voxels by Purss and Cull (2005) which has showed promise. Eskola et al. (1977) showed that since the potential U is a sum of the volume and surface pole distributions (σ_V and σ_S respectively), i.e.

$$U(\boldsymbol{R})=\int\sigma_V G(\boldsymbol{R})dV+\int\sigma_S G(\boldsymbol{R})dS\,, \tag{3}$$

then in a linear uniformly magnetized body where

$$\textbf{div}\,\boldsymbol{H}=-\textbf{div}\,\boldsymbol{M}=\sigma_V=0 \tag{4}$$

holds, one need only integrate over the body's surface. This method is used by Lee (1980) where a body is approximated with a number of facets.

This paper aims to: (1) introduce and test a prismatic sub-volume SDM scheme on simple bodies and test against the known results (i.e. for a sphere), (2) compare and investigate the accuracy and limitations of several different SDM correction schemes, (3) apply the prismatic sub-volume correction scheme to real data by modelling a dipping magnetite sheet, and (4) demonstrate the flexibility and generality of the sub-volume schemes by self-consistently modelling multiple magnetic bodies on the same grid.

METHOD AND RESULTS

We model a magnetic body with multiple prismatic sub-volumes after Sharma (1966). The *i*th component of the magnetic field from a prismatic volume are given by

$$H_i = \sum_k J_k \,.\, T_{ik} \qquad (5)$$

where T_{ik} is the Green's function for each source face and $\boldsymbol{J}_k$ is the magnetisation of the source. The total anomalous field including SDM effects may be calculated for a body by dividing it up into many prismatic (n) cells. The induced field at the centre of the mth cell is the sum of the primary inducing field and the field generated by all other sub-volumes i.e.

$$\boldsymbol{J}_m = \kappa \boldsymbol{H}_0 + \kappa \sum_n \sum_k \boldsymbol{J}_k \,.\, \boldsymbol{T}_{ik}\,. \qquad (6)$$

The number of cells required depends on the susceptibility and the geometry of the body to be modelled.

Simple bodies: Sphere

We first model a sphere with 136 cubes on a 41 cubed grid as shown in Figure 2. We use an inducing field of 60000 nT with an inclination of -60^0. Using (6) we calculate the magnetisation at the centre of each cube from the interactions with every other element. Within the volume we calculate that, as expected, ***div M*** ~ 0 and integrating over the surface of the body yields the field at each point within the 3D grid outside of the body. The results are shown in Figure 3 with North-South profiles over the centre of the top of the grid for different susceptibilities. The expected results for a sphere are plotted as pluses for three susceptibilities. The agreement between our calculated values and the analytic results is good and can be shown to improve with an increased grid resolution and/or number of sub-volumes.

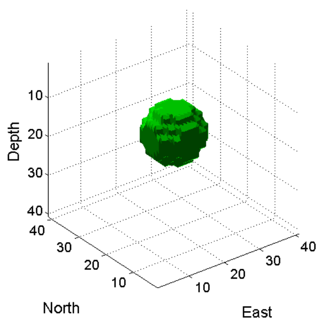

Figure 2. Sphere modelled with 136 sub-volume cubes on a 41 cubed 3D grid.

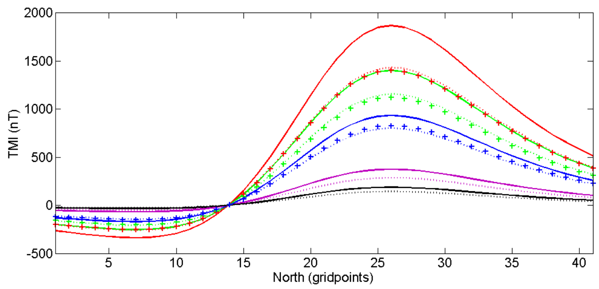

Figure 3. A North/South profile over a modelled sphere for different magnetic susceptibilities. The susceptibilities are equal to 1 for the red line, 0.75 for the green line, 0.5 for the blue line, 0.2 for the purple line, and 0.1 for the black line. The dotted lines show the fields corrected for SDM. The pluses show the expected field using the spheres demagnetisation factor for three different susceptibilities.

Simple bodies: Cube

Next we model a cube with κ=1 to test the prismatic sub-volume scheme, the spherical voxel scheme of Purss and Cull (2005), and a commercial modelling software package ModelVision. The spherical voxel scheme relies on dividing a body up into many sub-volume spheres and iteratively computing the field interactions of the dipole sources (see Purss and Cull (2005) for details). The ModelVision approach is based on the multi-faceted surface integration method of Lee (1980). The input grids for the prismatic and spherical sub-volume scheme are shown in Figure 4 a) and b), respectively.

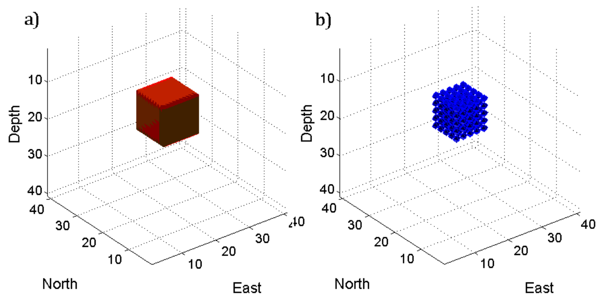

Figure 4. Cube modelled with 125 sub-volume cubes on a 41 cubed 3D grid using a) cubes and b) spheres.

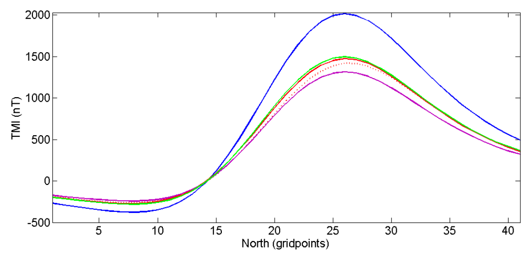

Figure 5. A North/South profile over a modelled cube using different SDM correction schemes. The blue line is the anomalous field without any correction, the green line is the corrected field using the spherical voxel scheme, the red line is the corrected field using the prismatic scheme with the surface contributions only (dotted line) and the surface and volume contributions (solid line), and the purple line is the corrected field using ModelVision.

The results are summarised in Figure 5 for the three different correction schemes. As per above, the demagnetising factor for a cube of κ=1 is 1/3, and therefore the field should be reduced by 75%. Both the spherical and prismatic sub-volume schemes agree well with each other and to within 1% and 2% of the known values, respectively, when the volume contributions are included in the prismatic calculation. Although the volume pole contributions are small compared to the surface pole contributions, edge effects in the modelling mean that ***div*** $M \neq 0$. Integrating only over the surface for the prismatic scheme brings it closer to the corrected field found using ModelVision which is within around 10% of the correct solution.

Complex bodies: Case study

To demonstrate the method and to investigate SDM effects we apply the prismatic scheme to a more complex dipping sheet body that is used to model an anomaly over a magnetite mine North-East of Albany in Western Australia. The data and location are shown in Figure 5. Here the inducing field has a strength of 59700 nT with a declination of -1.3^0 and an inclination of -69^0.

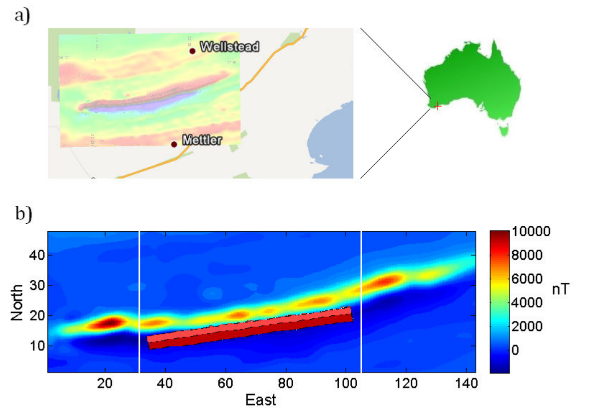

Figure 5. Aeromagnetic data of a magnetic anomaly North-East of Albany, Western Australia. a) The anomaly is shown in context as a histogram equalised colour contour plot. b) The anomaly of interest has been cropped and plotted on a 143x48 grid where the colour represents the total magnetic field intensity. Each grid point is approximately equal to 80m. The anomaly between the white markers is modelled as a dipping sheet (top shown in red).

We first use ModelVision to perform an inversion on a line of data running approximately North-South and model it as a dipping sheet both without and with the facet SDM approximation applied. The dimensions of the two solution bodies are quite similar being approximately 170m thick, 17m to 900m deep, a strike length of 5.5 km, and a strike azimuth of 82^0. The main difference between the two solution bodies is the susceptibility and the southward dip, being κ=0.77 vs. κ=1.25, and 74^0 vs. 77^0 for the inversion without and with the SDM correction effects applied, respectively. The profile of the line data and the solution bodies is displayed in Figure 6.

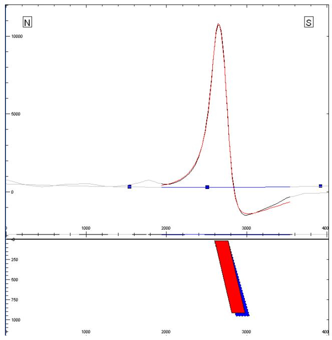

Figure 6. Approximately North-South (left to right) magnetic line profile (black line) showing the fit to the data generated by the two solution bodies (red line). The red sheet was modelled without SDM effects (κ=0.77) while the blue sheet was modelled with SDM effects (κ=1.25). The horizontal extent North-South here is approximately 4km.

The sheets are modelled in a 61 cubed grid point volume using approximately 1000 cubes (each cube representing ~100m^3) as shown in Figure 7 a). The simulation grid is centred between the vertical white lines in Figure 5 b). The results for the first body (κ=0.77) modelled with no SDM results are shown in Figure 7 b) as a contour plot. Due to the coarse resolution of the grid, the stepped cubes in the modelled sheet are visible in the field results. Furthermore, to achieve an observation height similar to the flight line height (plus depth to the top surface of the body) in the data in Figure 5, an average was taken between 50m and 150m above the body's surface in Figure 7 b). Nonetheless, the levels in the total magnetic intensity agree quite well and increasing the grid resolution and/or number of sub-volumes should improve this agreement.

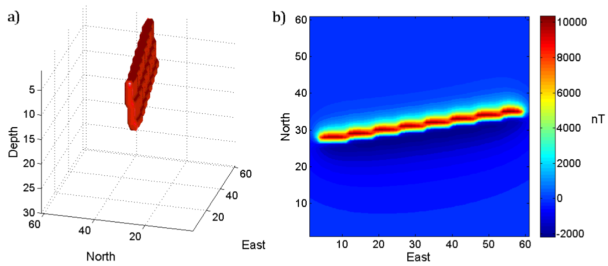

Figure 7. a) Red sheet from Figure 6 modelled using 1008 sub-volume cubes on a 61 cubed 3D grid. b) Contour plot of total magnetic intensity at the average of 50m and 150m above the modelled body (κ=0.77). Each gridpoint = 100m.

The SDM effects are calculated for both the high and low susceptibility bodies with the results plotted in Figure 8 as the total magnetic intensity as a function of distance. This plot illustrates the difference in results when correction for SDM is considered. Whilst the body with the lower susceptibility explains the anomaly without a correction applied (as in Figure 7 [b]), in reality the anomalous field would be suppressed by demagnetisation effects. Our modelling shows these effects to be around 10% and 28% for the body with low and high susceptibility, respectively. It also demonstrates qualitative agreement between the prismatic sub-volume scheme results and those obtained with ModelVision. However, there is a quantitative difference in results when comparing the solid red and dotted blue line in Figure 8, which are equal when modelled in ModelVision (as in Figure 6).

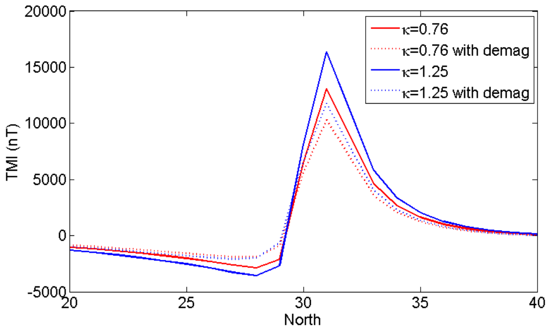

Figure 8. North-South line over the middle of the 3D grid modelling the dipping magnetite sheet. Each grid point = 100m.

Multiple bodies of arbitrary geometry

The main advantage of the prismatic sub-volume technique is now demonstrated by self-consistently modelling multiple magnetic bodies in the same grid. We are not aware of any commercially available software packages that are able to calculate the demagnetisation effects of multiple body interactions. Figure 9 shows three bodies, two dipping sheets and a prism, modelled using ~5000 cubes in total with κ=1 and the same inducing field as used for the simple body modelling above . The total magnetic intensity calculated at the top of the 3D grid is shown in Figure 10 a) and b), both without and with SDM effects taken into account, respectively. The intensity of the image in Figure 10 b) is clearly suppressed compared with Figure 10 a). This demonstrates strong inter-body and intra-body demagnetisation effects since the field suppression is stronger than that of each body modelled in isolation, and the resultant contour image is distorted and more spread out.

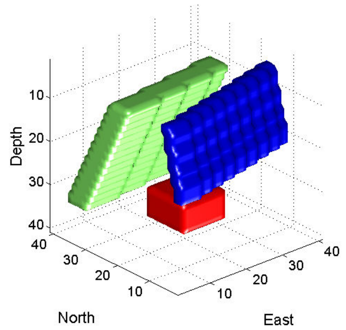

Figure 9. Multiple magnetic bodies (κ=1) modelled in a 41 cubed 3D grid.

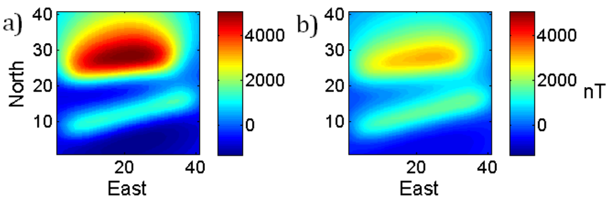

Figure 10. Contour plots of total magnetic intensity at the top of the grid for a) no SDM correction, and b) SDM correction applied.

CONCLUSIONS

The sub-volume schemes show good accuracy when compared with the known results for simple bodies, even when modelled on coarse grids. Typically the calculated results were within a few percent of the known solutions. While the results are slow to compute compared with approximations made by ModelVision for example, the results should more correctly account for SDM effects in bodies with complex geometries given a fine enough grid resolution. Furthermore, the interactions between multiple bodies may be self-consistently modelled which cannot be done in commercially available software packages.

Future work will include extending the investigation to model bodies with non-uniform susceptibilities, which is a unique extension of the sub-volume approach. Comparisons between the computed SDM effects for multi-body anomalies will also be a useful investigation for the correction schemes. Finally, we plan to implement an iterative data/modelling comparison scheme to provide a means of forward modelling and inversion.

ACKNOWLEDGMENTS

Thank you to David Clark for suggesting and providing helpful literature on the subject.

REFERENCES

Clark, D.A., Saul, S.J., and Emerson, D.W., 1986, Magnetic and gravity anomalies of a triaxial ellipsoid: Exploration Geophysics, 17, 189-200.

Emerson, D.W., Clark, D.A., and Saul., S.J, 1985, Magnetic exploration models incorporating remanence, demagnetisation and anisotropy: HP 41C handheld computer algorithms: Exploration Geophysics, 16, 1-122.

Eskola, L., Tervo, T., and Puranen, R., 1977, Calculation of magnetostatic anomalies and demagnetization factor by means of the method of subareas: Geological Survey of Finland, Report of Investigation No. 16.

Lee, T.J., 1980, Rapid computation of magnetic anomalies with demagnetization included, for arbitrary shaped magnetic bodies: Gephysical Journal of the Royal Astronomical Society 60, 67-75.

Purss, M. And Cull, J., 2005, A new iterative method for computing the magnetic field at high magnetic susceptibilities: Geophysics 70(5), 53-62.

Sharma, P.V., 1966, Rapid computation of magnetic anomalies and demagnetization effects caused by bodies of arbitrary shape: Pure and Applied Geophysics 64(1), 89-109.